A unified topology approach to dot-, rod-, and sheet-MOFs

Chem

CellPress
OPEN ACCESS

Article

A unified topology approach to dot-, rod-, and sheet-MOFs

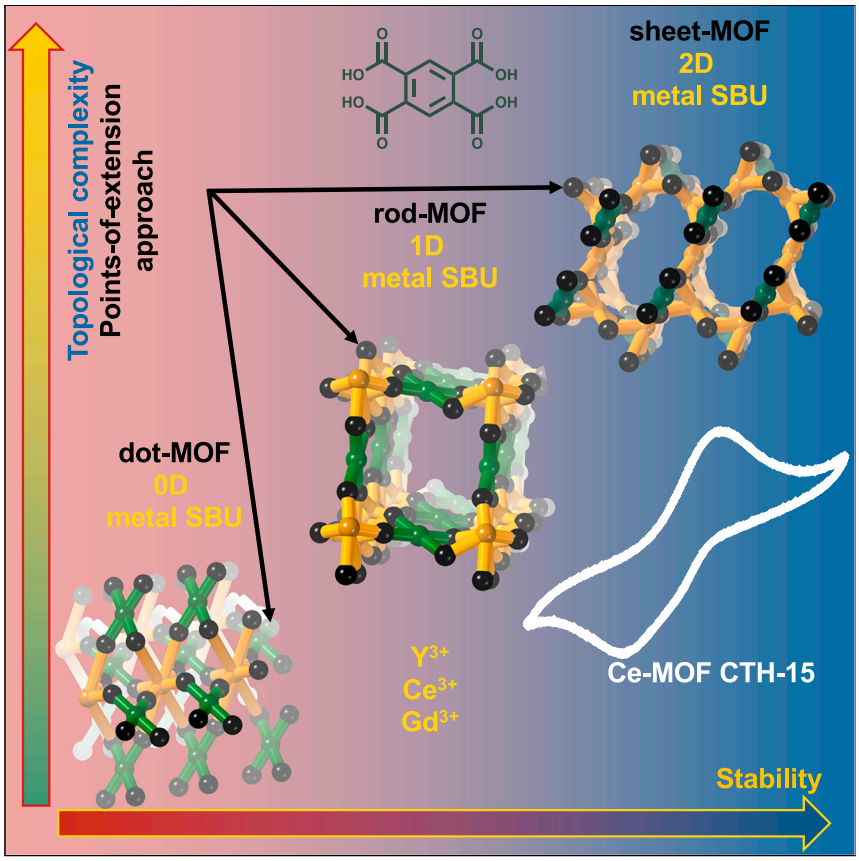

We offer insights into how network topology influences stability of metal-organic frameworks and suggest the application of rare sheet-MOFs, where metal ions and linkers form infinite 2D units (SBUs) as a strategy for achieving higher stability. We also demonstrate a unified topology approach to MOFs exemplified by the dot-, rod-, and sheet-MOFs reported. These MOFs are based on vicinal dicarboxylates, which we propose as a way to prepare rod-MOFs. Cyclic voltammetry suggests Ce(IV)-MOFs as being more stable than expected with potential electrochemical applications.

Francoise M. Amombo Noa, Maria Abrahamsson, Elisabet Ahlberg, Ocean Cheung, Christian R. Göb, Christine J. McKenzie, Lars Öhrström

mystere@chalmers.se (F.M.A.N.)
ohrstrom@chalmers.se (L.Ö.)

Highlights

Metal-organic frameworks split into dot-, rod-, and sheet-MOFs based on the metal units

The stability of MOFs follow the trend sheet-MOF > rod-MOF > dot-MOF

A unified topological network analysis uses carboxylate C:s as points of extension

Electrochemistry shows cerium(IV) stabilized in MOFs

Amombo Noa et al., Chem 7, 2491–2512
September 9, 2021
Published by Elsevier Inc.
https://doi.org/10.1016/j.chempr.2021.07.006

Chem

CellPress
OPEN ACCESS

Article

A unified topology approach to dot-, rod-, and sheet-MOFs

Francoise M. Amombo Noa,[1,*] Maria Abrahamsson,[1] Elisabet Ahlberg,[2] Ocean Cheung,[3] Christian R. Göb,[4] Christine J. McKenzie,[5] and Lars Öhrström[1,6,*]

SUMMARY

Metal-organic frameworks made from multi-metal-ion units in the shape of clusters and rods (termed dot-MOFs and rod-MOFs) are well known. Here, we introduce MOFs with multi-metallic units in the form of sheets—sheet-MOFs. We show exemplars of all three types of units based on structures containing Y^{3+}, Ce^{3+}, or Gd^{3+} linked by benzene-1,2,4,5-tetracarboxylate to give crystals of a dot-MOF in H_2NMe_2[Y(btec)(H_2O)] CTH-14, a sheet-MOF in [Ce_3(btec)(Hbtec)(OAc)(HCO_2)] CTH-15, and a rod-MOF in 4,4′-azopyridinium[Gd_2(btec)$_2$] CTH-16. Cyclic voltammetry shows that CTH-15 stabilizes Ce(IV). Given the fact that sheet-MOFs represent an intellectual advance in the evolution of MOFs, a unified approach is proposed for the topological classification of dot-, rod-, and sheet-MOFs. It is suggested that the stability of MOFs follow in the trend dot < rod < sheet. For CTH-14-16, the sheet- and the rod-MOF have higher thermal stability. We suggest sheet-MOFs as an additional strategy for making robust MOFs.

INTRODUCTION

The assembly and structure-directing role of the multi-metallic secondary building unit (SBU) is central to the synthesis and understanding of metal-organic frameworks (MOFs).[1] In most cases, the metal-containing SBU can be reduced to a single point, 0D (for example {$Zn_4O(OCO)_6$} in MOF-5) with a certain geometry (octahedral in MOF-5) and connectivity (6-c) to the organic SBUs. We will refer to this as a dot-MOF. In some MOFs, however, carboxylates, imidazolates, or other Lewis base groups bridge the metal ions in an infinite pattern where it is not possible to define a 0D SBU (Figure 1 center and right). Most notably, we find these in the rod-MOFs, where the metal ions are connected to form an infinite 1D SBU, such as {$Mg_2(O-CO)_2(O)_2\}_\infty$ in MOF-74, then further connected into a 3D framework by the organic SBUs.[2] In this report, we introduce the concept of infinite 2D SBUs. To date, these are rare in MOF chemistry, but our findings indicate that they are important. We will refer to them as sheet-MOFs, and the three classes are compared in Figure 1.

For some MOF applications, the stability, chiefly thermal or resistance to degradation in solution[3] (i.e., water at high or low pH) as well as mechanical stability, will be a crucial parameter for real-world devices. Although there are no comprehensive systematic stability studies of a large sampling of different MOFs, indications are that rod-MOFs are more thermally stable than dot-MOFs.[4] We note that the rod-MOF topology was recently credited with the hydrolytic stability of the water-harvesting MOF-303,[5] and that the rod-MOF MFM-300(Cr) was recently branded as "ultrastable."[6]

By analogy, we suspect that sheet-MOFs are even more stable than rod-MOFs, principally because the higher the dimensionality of the SBU, the less likely it is to have a strained structure especially around the metal sites.

The bigger picture

Metal-organic frameworks is an emerging class of materials with wide-ranging capabilities due to tunability, high surface area, porosity, and large internal void spaces. However, stability may be an issue. Here, we argue for increased stability going from discrete multi-metal entities to infinite rods to sheets as building units and propose a unified way to classify them.

We present a rare sheet-MOF based on non-dense 2D net, opening the way to even more stable MOFs while preserving the potential of high porosity and surface area. Cyclic voltammetry on this Ce(III)-based MOF CTH-15 indicates a remarkable stabilization of the Ce(IV) oxidation state and that more Ce(IV) MOFs may be feasible. Potential applications of this, or similar MOFs, in electrochemical applications related to drinking water purification are discussed.

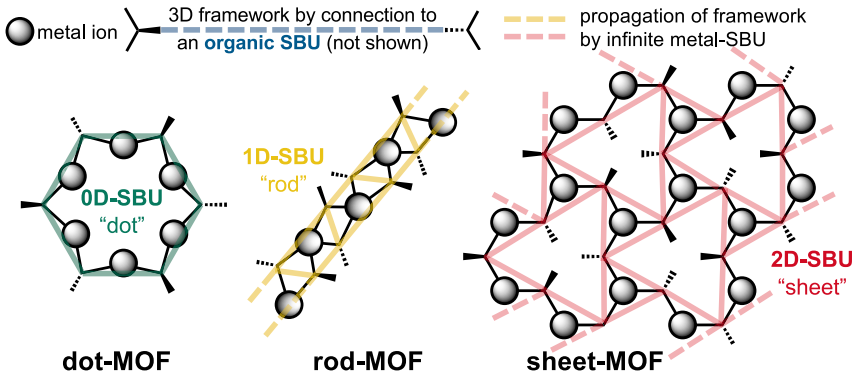

Figure 1. Comparison of the three classes of MOFs based on metal SBUs

Left: Dot-MOF built from discrete metal-ion entities (0D) as small as a single-metal ion up to 2-figure numbers. Center: Rod-MOF with 1D infinite metal SBU. Right: Sheet-MOF with 2D infinite SBU. In all cases, the organic SBUs (not shown) connect the metal SBUs to a three-dimensional framework. For clarity, only the SBUs are shown, not the 3D framework.

For thermal tolerance, the sheet-MOF performance is indicated by the remarkable stability of ULMOF-1, up to 610°C under a nitrogen atmosphere.[7] In this compound, sheets of edge- and corner-shared lithium-oxygen tetrahedra connect to a dense sheet bridged by 1,4-benzene dicarboxylate (bdc) organic SBUs. Another example is the Na^+-based MOF-705 and MOF-706. Their sheet-MOF properties were used to explain the unusual stability.[8]

There are good reasons to be observant of this general classification. However, a more precise description of topologies is essential in reticular chemistry synthesis planning,[1] analysis, and communication of the resulting structures.[9–13] Properties such as porosity and flexibility have recently been investigated using the topology approach,[14] and a special case of folding topologies has been identified.[15] However, rod-MOFs, and now sheet-MOFs, pose a particular problem because these are commonly analyzed in a different way from dot-MOFs.[2,16,17] A unified approach would be advantageous both from a synthesis and an understanding perspective. Note, however, we do not in any way seek to supersede or diminish current efforts to generate solid algorithms for the automatic analysis of the large amount of crystallographic data now available[18,19]; we find these absolutely essential.

We approach the topology question from the vantage point of three MOFs prepared with benzene-1,2,4,5-tetracarboxylate, H_4btec: a dot-MOF in H_2NMe_2[Y(btec)(H_2O)] **CTH-14**, a sheet-MOF in [Ce_3(btec)(Hbtec)(OAc)(HCO_2)] **CTH-15**, and a rod-MOF in 4,4′-azopyridinium[Gd_2(btec)$_2$] **CTH-16**. From the MOF design point of view, we note that btec, with its vicinal 1,2-dicarboxylates, seems prone to form rod-MOFs, and this synthesis strategy will be elucidated further. As for rare-earth-element (REE)-based MOFs, these are fascinating for their luminescence properties, and the high coordination numbers of the REE ions make for diverse geometries and unprecedented network topologies.[20] Moreover, H_4btec is luminescent on its own, and we report on how this property is modulated by the REEs in these solids.

More importantly, MOFs have been identified as catalysts for different reactions related to environmental issues.[21] Specifically, Ce-MOFs were demonstrated as

[1]Division of Chemistry and Biochemistry, Department of Chemistry and Chemical Engineering, Chalmers University of Technology, 412 96 Gothenburg, Sweden

[2]Department of Chemistry & Molecular Biology, University of Gothenburg, 405 30 Gothenburg, Sweden

[3]Nanotechnology and Functional Materials, Department of Material Sciences and Engineering, Uppsala University, 751 21 Uppsala, Sweden

[4]Rigaku Europe SE, Hugenottenallee 167, 63263 Neu-Isenburg, Germany

[5]Department of Physics, Chemistry and Pharmacy, University of Southern Denmark, Campusvej 55, 5230 Odense M, Denmark

[6]Lead contact

*Correspondence: mystere@chalmers.se (F.M.A.N.), ohrstrom@chalmers.se (L.Ö.)

https://doi.org/10.1016/j.chempr.2021.07.006

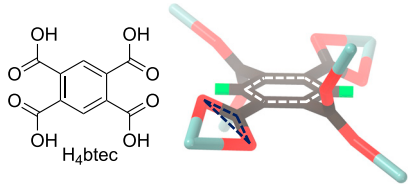

Figure 2. Benzene-1,2,4,5-tetracarboxylic acid H_4btec and bonding to REE M^{3+}
Note the angles between the carboxylate group and the benzene plane (dashed lines) that are further investigated in Figure 6. The (H_4btec) ligand offers two carboxylate groups in close vicinity and therefore may be prone to the formation of infinite SBUs.

effective catalysts for combustion of volatile organic compounds in air,[22] and Ce(IV/III)-MOF catalysis was recently proposed for hydrolysis of nerve agents.[23] We have investigated the redox properties of the Ce- and Gd-MOFs **CTH-15** and **CTH-16** by cyclic voltammetry, and our results suggest a stabilization of Ce(IV), normally a strong oxidant.

Benzene-1,2,4,5-tetracarboxylate, H_4btec (Figure 2) is a somewhat odd MOF linker because the two carboxylate groups on each side are in close proximity. This looks inviting for synergistic coordination in which the metal-ion attachment to one carboxylate influences the coordination of the second one. There are 350 such MOFs or coordination networks reported in the Cambridge Crystallographic Database (CSD) to date, starting with a Ce(III)btec compound in 1997.[24]

RESULTS AND DISCUSSION

We start with synthesis and structures, then move on to thermal characterization, chemical stability, photoluminescence, and electrochemical properties. In the final part, the discussion draws from all these parts, touching on synthesis, flexibility, and topology. Figure 3 gives an overview of the structures of **CTH-14**–**CTH-16**.

Synthesis and structures of CTH-14, CTH-15, and CTH-16

The solvothermal reaction of H_4btec, 4,4′-azopyridine and $Y(NO_3)_3 \cdot 6H_2O$ in a 1:1:2 (v/v/v) DMF/H_2O/glacial acetic acid solution in a pyrex tube at 120°C produced colorless single crystals of **CTH-14**, $H_2NMe_2[Y(btec)(H_2O)]$ after 24 h. A similar method was applied in the making of **CTH-15**, $[Ce_3(btec)(Hbtec)(OAc)(HCO_2)]$ and **CTH-16**, 4,4′-azopyridinium$[Gd_2(btec)_2]$ with the exception that the metal salts were $Ce(NO_3)_3 \cdot 6H_2O$ and $Gd(NO_3)_3 \cdot 6H_2O$, respectively. In **CTH-15**, colorless crystals were obtained after 3 days, and pale yellow crystals of **CTH-16** were acquired on the second day of the solvothermal reaction. **CTH-14** and **CTH-15** could also be prepared without the presence of 4,4′-azopyridine.

Table S1 details the crystallographic data and structure refinement parameters of **CTH-14**, **CTH-15**, and **CTH-16**, and we also comment on the refinement processes of **CTH-15** and **CTH-16**. A short summary of the crystallography is provided below. Figures S1–S5 give some more detail of the structures.

When the structures are discussed, it will be clear that neither of these compounds are expected to show any remarkable surface areas or porosities. The gas sorption results are therefore only briefly presented and discussed after each structure. More details are provided in Table S6.

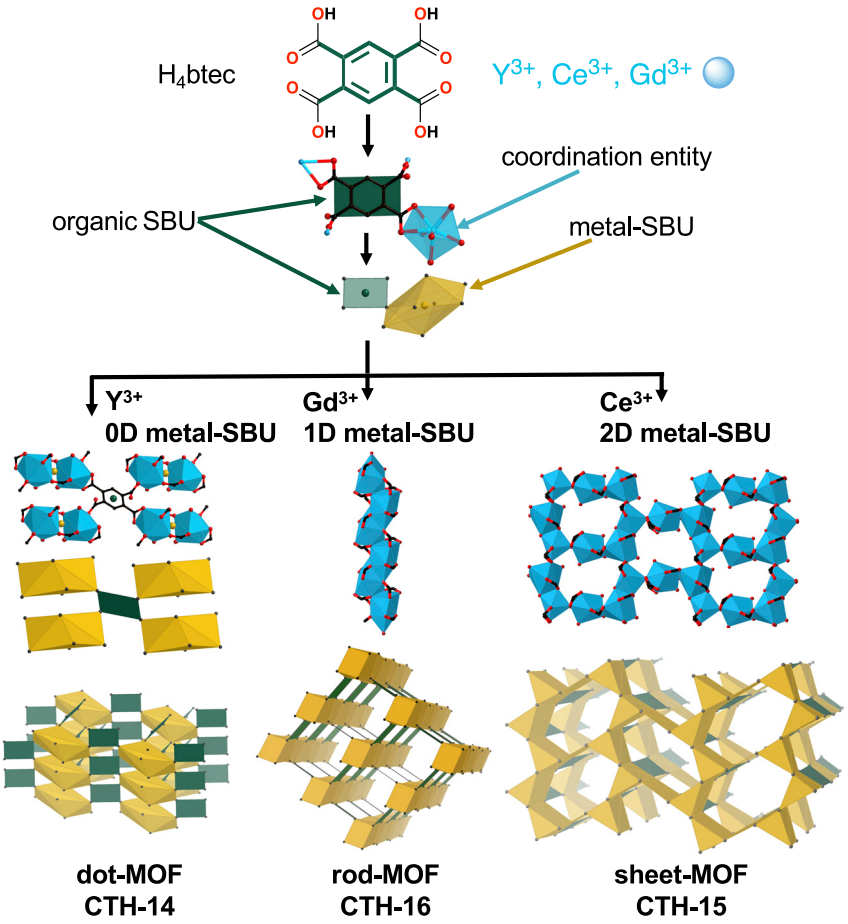

Figure 3. Overview of the three different MOFs, CTH-14, CTH-15, and CTH-16

The MOFs were obtained using solvothermal conditions from H_4btec and mononuclear metal precursor salts in DMF with or without the 4,4′-azopyridine (except **CTH-16**). This gives MOFs with the same organic SBU (btec part shown in green) and three distinct carboxylate-bridged coordination entities (shown in cyan), which in turn can be thought of as a 0D metal SBU and infinite 1D or 2D metal SBUs. This gives one dot-MOF, one rod-MOF, and one sheet-MOF whose network topologies were analyzed. Green and yellow spheres indicate nodes in the 0D SBUs, and black spheres nodes in the network using the points-of-extension approach (*vide infra*). More details are given below and in Figures S1–S4.

$H_2NMe_2[Y(btec)(H_2O)]$: CTH-14

$H_2NMe_2[Y(btec)(H_2O)]$ crystallizes in the $P\bar{1}$ space group with an asymmetric unit consisting of one Y ion, one btec linker, one dimethylammonium cation ($H_2NMe_2^+$), and one H_2O molecule coordinated to Y. The coordination network in **CTH-14** is a straightforward dot-MOF (Figure 3), although the dimethylammonium ions fill most of the potential voids in the structure. Y^{3+} binds to five $btec^{4-}$ and the $btec^{4-}$ binds to either 4 or 6 Y^{3+}. The coordination sphere of Y^{3+} is completed by one water molecule to give coordination number 8. The framework is stabilized by hydrogen bonds (Table S2) between btec, H_2O, and $H_2NMe_2^+$.

As expected, this compound shows no porosity in the gas sorption experiment.

$[Ce_3(btec)(Hbtec)(OAc)(HCO_2)]$: CTH-15

All tested crystals of **CTH-15** had similar lattice constants and were potentially pseudo-merohedral twinned. This compound, whose structure solved in the monoclinic space

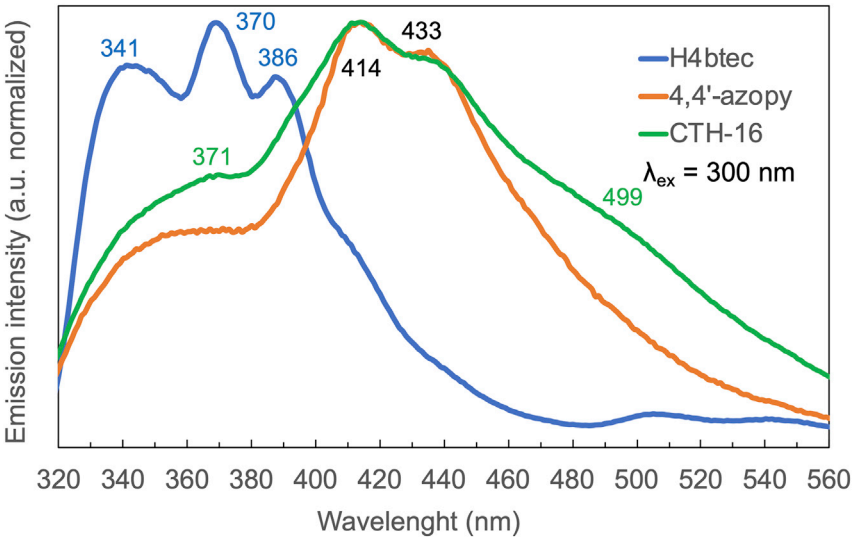

Figure 4. Normalized solid-state photoluminescence spectra of CTH-16, H_4btec, and 4,4′-azopyridine

The solid-state luminescence (λ_{exc}= 300 nm) of **CTH-16** is dominated by the luminescence from the guest molecule 4,4′-azopyridine resident in the framework voids. Intensities are in arbitrary units, normalized, and cannot be directly compared. For other luminescence spectra, see Figures S25 and S26.

group $P2_1/c$ with a very small monoclinic angle of 90.011(2)°, has three symmetry-independent Ce atoms, bonding 10–12 oxygen atoms each, and two btec ligands in different protonation states, a common occurrence for Ln-btec-MOFs. Formate is a common breakdown product of the DMF solvent and acts as a non-bridging, coordinating anion.

This Ce-MOF has an unusual network for a MOF in that an infinite 2D SBU is formed (Figure 3). The calculated porosity of **CTH-15** with solvent removed is 38% with spherical cavities of diameter 4.2 Å using CrystalMaker (see supplemental information for details) or 20.7% using the more common Platon approach. However, neither the porosity by N_2 sorption at liquid N_2 temperature nor CO_2 and N_2 sorption at ambient temperature (20°C) could be verified possibly because channel diameter may be too narrow to detect,[25] or, as indicated by a solvent accessible void calculation, the voids are more isolated cavities than channels (see supplemental information for details). Powder diffraction indicates that **CTH-15** retains its network structure after activation in vacuum and the gas sorption experiment.

4,4′-azopyridinium[Gd_2(btec)$_2$]: CTH-16

4,4′-azopyridinium[Gd_2(btec)$_2$] **CTH-16** crystallizes in the triclinic space group $P\bar{1}$ with its asymmetric unit containing one nine-coordinated Gd center, two half btec linkers, and one half 4,4′-azopyridium. In analogy with the isoreticular series (4,4′-bipyridinium)[Ln_2(btec)$_2$] Ln = Pr, Eu, Gd,[26] we assign the missing charges to protonated pyridine (O4…H-N4 2.394 Å) rather than a protonated btec ligand based on their presumed pK_a values although the proton cannot be identified from the electron density map. The 4,4′-azopyridinium ion itself is situated around a special position in the channels of **CTH-16**. It was isotropically modeled as a fragment obtained from CSD structure KUGJUS[27] because it is disordered, which is frequently the case. Of 152 structure determinations in the CSD with organic co-crystals of 4,4′-azopyridine, more than 40% display disorder or other problems. The identity of the 4,4′-azopyridinium guest was moreover confirmed by luminescence measurements (Figure 4). There are no apparent voids in the structure,

and gas sorption measurements did not show any porosity for this compound. As shown in Figure 3, **CTH-16** is a typical example of a rod-MOF.

Having established the structures, we now investigate some properties of these materials.

Thermal analysis, thermal stability, and powder X-ray diffraction

CTH-14–CTH-16 were studied by thermogravimetric analysis (TGA) under air and exhibited different thermal behaviors. In the thermogravimetric curve of **CTH-14** (Figure S12), the first two mass losses were associated to the loss of the dimethylamine ($HNMe_2$) (found 10.4%, calculated 11.2%); the rest corresponded to the loss of the coordinated water molecule and the decomposition of the linker (btec). The **CTH-15** TGA curve is illustrated in Figure S13 and shows a first weight loss at 8.80%, which is the release of mass corresponding to solvent (calculated 8.1%). The second weight loss indicates the decomposition of the linker, acetate, and formate to give a residue of 47.7% CeO_2 (calc. 46.0 %). TGA analysis of **CTH-16** (Figure S14) gave one weight loss, which means that 4,4′-azopyridinium is tightly held in the **CTH-16** pores.

Although constant weight during a TGA experiment is no proof of architectural stability, it is still an indication of the material's overall thermal stability.[4] For our compounds, the onset of thermal degradation is clearly some 20° lower for **CTH-14** compared with **CTH-15–CTH-16** that show close to identical starting points of the mass loss at around 400°C. This is consistent with the idea that rod- and sheet-MOFs are more stable than dot-MOFs such as **CTH-14**.

The PXRD patterns of **CTH-14–CTH-16** were in good agreement with their calculated PXRD patterns, as demonstrated in Figures S15–S17. PXRD patterns of these three MOFs were collected after N_2 sorption experiments, indicating that all samples remain intact after activation except for **CTH-16**. PXRD was further used to explore the thermal architectural stability of the materials (Figures S18–S20).

Heating up to just under the decomposition temperature as indicated by the TGA experiment, 350°C, shows the dot-MOF **CTH-14** losing architectural integrity and transforming to another unknown crystalline phase already after the 120° vacuum activation for the gas sorption experiment. The sheet-MOF **CTH-15** and rod-MOF **CTH-16** on the other hand are stable up to at least 350°C.

The compounds do differ in some substantial ways other than the dimensionality of the SBUs, so to make the case for a stability trend dot < rod < sheet, we need to look at more data. Recently, Bennett and co-workers[4] reported a study of MOF thermal stability. They based their analysis on the onset of decomposition from the plateau phase in the TGA, and more than 200 MOF TGA experiments were taken into account. We picked out and analyzed the topology of the metal SBUs for the most stable MOFs in this study with a T_d exceeding 500°C (see Table S4).

We found that of these 10 thermally stable MOFs, there were one dot-MOF, six rod-MOFs, and three sheet-MOFs, with the sheet-MOF ULMOF-1 taking the record, being stable up to 610°C as already mentioned. Although this corroborates our idea, we acknowledge that this cannot be the only factor deciding the thermal stability.

In this respect, we note that the only MOFs stable enough to melt are a couple of ZIFs. ZIF-4 melts at 567°C and ZIF-62 at 410°C and is stable for another 100°C.[28]

This seems understandable in light of the above discussion as ZIFs connected only through their imidazolate units can be thought of as having three-dimensional SBUs.

Chemical stability

Chemical stability of **CTH-14**, **CTH-15**, and **CTH-16** were probed by soaking the MOFs in water at pH 7, aqueous 5-M HCl, and aqueous 5-M NaOH at room temperature for 1 h (Figures S21–S23). All three MOFs were stable in water for at least 1 h, as their corresponding PXRD patterns remained the same as the as-synthesized products. In 5-M HCl, **CTH-14**, **CTH-15**, and **CTH-16** maintained their crystallinity although some peak broadening was observed, but their final products did not match their as-synthesized diffraction patterns but rather H_4btec on its own (Figure S24). Lower chemical stability of these three MOFs were found when using very basic (5-M NaOH) media. There is loss of intensity in the PXRD patterns of **CTH-14** and **CTH-16** and a rather amorphous final product in **CTH-15**. This is likely because **CTH-15** has a relatively good leaving group (formate, pK_a 3.7), which is easily attacked and may provoke the decomposition of the framework (the exchange of formate for other anionic molecules has been demonstrated in, for example, MOF-520[29]).

Ding et al.[3] recently surveyed solution-stability studies of MOFs, and again, we picked the most stable examples, materials reported to survive a week or more under various conditions (see Table S3). Of these, eight are dot-MOFs, another eight rod-MOFs, and one is a ZIF, thus with a 3D SBU. We note that of these, only ZIF-8, MIL-177-LT, and two rod-MOFs were stable under as harsh conditions as we tested **CTH-14**, **CTH-15**, and **CTH-16**.

Again, given the predominance of dot-MOFs, this supports that the dimensionality of the metal SBU is a factor also in solution stability. The importance of chemical stability in many chemical applications of MOFs makes it somewhat surprising to note the scarcity of thermodynamic solubility product data.[30]

Photoluminescence properties

Lanthanoid-based MOFs have become popular in the past years because of their potential useful magnetic and photoluminescence properties. These properties are attributed to their geometries, higher coordination numbers compared with transition metals, inherent luminescent abilities, and high number of unpaired electrons.[31–33] The luminescence properties of **CTH-14**, **CTH-15**, and **CTH-16**, H_4btec, and 4,4′-azopyridine were investigated in the solid state at room temperature using an excitation wavelength of 300 nm. Detailed assignments are discussed in the supplemental information.

The emission spectra of the free ligands are displayed in Figure 4. H_4btec exhibits somewhat structured emission at 370 nm in line with previous studies,[34,35] while 4,4′-azopyridine on the other hand shows a less structured emission band at 414 nm.[36]

The photoluminescence spectrum of **CTH-14** shows emission at 351 nm, whereas **CTH-15** has a more intense emission at 400 nm, both consistent with similar compounds[37,38] (Figure S25).

The **CTH-16** spectrum (Figure 4) is dominated by an emission band at 414 nm, which can be attributed to the 4,4′-azopyridine guest. Weaker features at around 370 and 500 nm are also observed that may originate in the btec ligand (Figure S26). This

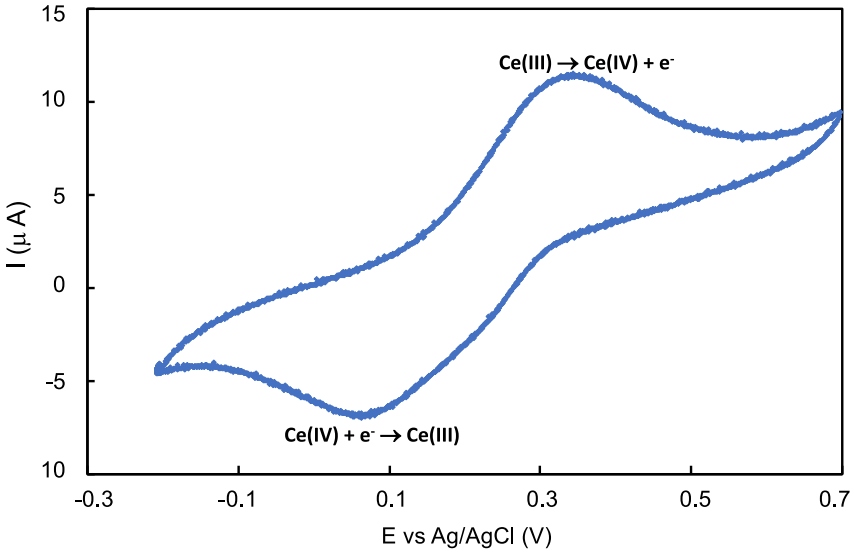

Figure 5. Cyclic voltammetry of the Ce(IV)/Ce(III) redox couple in CTH-15

Cyclic voltammogram of **CTH-15** in carbon paste, 0.1 M phosphate buffer, pH = 7 and sweep rate 10 mVs^{-1} showing that the redox potential of Ce(IV)/Ce(III) in [Ce_3(btec)(Hbtec)(OAc)(HCO_2)] **CTH-15** is about 0.2 V versus Ag/AgCl, a remarkable stabilization of Ce(IV) compared with the aqueous solution chemistry. For other cyclic voltammograms, see Figures S27 and S28.

indicates that 4,4′-azopyridine is present in the **CTH-16** structure, corroborating the findings from the X-ray investigation. However, these measurements do not appear to be sensitive to whether the 4,4′-azopyridine is coordinated to a metal ion or protonated.[39]

Compounds **CTH-14**, **CTH-15**, and **CTH-16** exhibit photoluminescent behaviors that may warrant further investigations in light of the need for devices stable to moisture, air, and thermal degradation,[40,41] especially given the architectural stability of **CTH-15** up to 350°C as shown by powder diffraction and the insolubility in common polar and non-polar solvents.

Electrochemistry

The electrochemical behavior of **CTH-15** and **CTH-16** was characterized by cyclic voltammetry in the solid state using a carbon paste electrode.

For **CTH-15**, the voltammogram shows a quasi-reversible electron transfer reaction, probably related to the Ce(IV)/Ce(III) redox couple in the MOF structure, see Figure 5 (as no corresponding couple was shown for **CTH-16** with the non-redox active Gd^{3+}). The electron transfer kinetics is slow as expected for a carbon paste electrode. The redox potential is about 0.2 V versus Ag/AgCl, taken as the mean value between the anodic and cathodic peak potentials.

For the Ce(IV)/Ce(III) in aqueous solution, the reversible potential is 1.72 V versus SHE, i.e., 1.52 V versus Ag/AgCl.[42] The large decrease in oxidation potential for **CTH-15** means that Ce(III) is destabilized in the structure, i.e., it is more easily oxidized, whereas Ce(IV) is stabilized and more difficult to reduce than its corresponding water complexes. This is in line with previous solution studies indicating a substantial span in redox potentials for the Ce(IV)/Ce(III) couple and in particular stabilization of the Ce(IV) by anionic oxygen ligands.[43,44] Notably, with the

octadentate 1-hydroxy-2-pyridinonate ligand 3,4,3-li-(1,2-hopo), the Ce(IV)/Ce(III) potential was measured to be 0.175 V versus Ag/AgCl,[45] close to the Ce(IV)/Ce(III) potential measured for **CTH-15**. It is also in line with very recent studies on Ce(IV)-MOF-808.[46]

Cerium is well established in various electrochemical processes,[47] but studies of electrochemical applications of MOF have been mostly concentrated on batteries and supercapacitors or water-splitting reactions.[48] Given the affinity of cerium ions to nitrate ions,[47] it would be interesting to explore **CTH-15** or related systems in catalytic electrochemical nitrate reduction, an important issue due to a pressing need to remove nitrate from drinking water.[49,50] We note that the general requirements for a nitrate reduction cathode as pointed out by Zeng et al.[50] "liquid channels for reactant delivery and gas channels for product separation" seem to fit nicely with the MOF concept.[50,51] In this context, the low toxicity of cerium and its relative high earth abundance, on the level of copper, is noteworthy. More comprehensive studies of the electrochemistry of **CTH-15** and related systems are underway.

Gd(III) in **CTH-16** is not redox active, but the guest molecule 4,4′-azopyridine could in principle be reduced to the hydrazine. However, the two small redox couples that can be observed in the cyclic voltammogram of **CTH-16** (Figure S28) we tentatively attribute to the btec linker[52] because they have no resemblance to the electrochemical behavior of 4,4′-azopyridine, also investigated in the solid state (Figure S27), the latter showing two clear peaks for the oxidation and reduction, forming 1,2-di(pyridine-4-yl)hydrazine corresponding to the solution chemistry. This indicates that the guest is shielded in the structure and the reduction, requiring water or protons, cannot take place.

We will now discuss these results in a broader context.

Implications for btec-based MOF synthesis

Flexibility

The guests, or counter ions, are of slightly different shape and size in **CTH-16** and in the isoreticular (4,4′-bipyridinium)[Ln_2(btec)$_2$], meaning that the network has to have some flexibility. For the unit cell, this is expressed by 7% volume increase in **CTH-16** and a visibly less tilted network (Figure S4). There are many flexible, or "breathing" MOFs,[53–57] but the classic example is MIL-53,[58] a rod-MOF just like **CTH-16** with an **sra**-net. While there are different topological discussions of flexibility,[14,15] for MIL-53 and its derivatives, a kneecap movement of the metal carboxylates has been identified in the crystal structures. This involves bending of the M_2O_2 plane of the carboxylate versus the benzene plane, so that for a "closed" (GUSNEN01) version of MIL-53 the average angle is 30° and for the "open" (MINVOU) 10° (Figure S6 left).

In contrast, the out-of-plane turning of the carboxylates (Figure 2) is very slight for all such compounds, 85% laying within 22° from being co-planar and 10% being exactly co-planar (Figure S6 right). The situation is very different for the btec-MOFs, where there is a larger variety in angles and these angles are pairwise correlated (because of steric effects) (see Figure 6). We suggest that both of these mechanisms are in play simultaneously to render these frameworks flexible.

We also suggest that the flexibility of the btec ligand depicted in Figure 6 is partly responsible for the variety of structures observed with the REE ions. We count 17 different topologies in the 43 different 3D btec coordination polymers reported to date (Table S5).[14] Add to this around 10 2D compounds, and it is certainly a lot

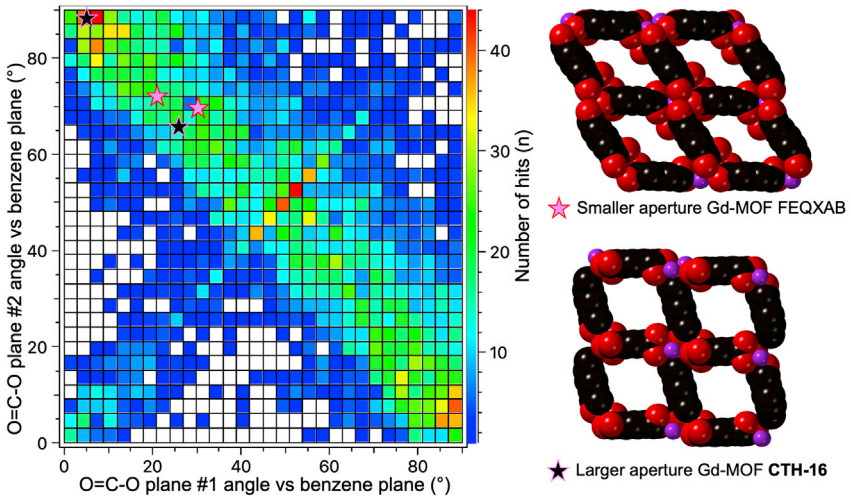

Figure 6. Analysis of vicinal benzene dicarboxylate structures in the CSD

Left: The structures of all vicinal (1,2) benzene dicarboxylates in the CSD were analyzed, and for each structure, the two angles between the carboxylate groups and the benzene plane were extracted (see Figure 2 for angle definitions). The many different angles may make both flexibility and a variety of network topologies possible. The potential energy surface also looks fairly flat. Values for **CTH-16** and the isoreticular Gd-btec-MOF with CSD code FEQXAB are indicated by stars. For a similar analysis of 1,4- benzene dicarboxylate-based MOFs, see Figure S6. Right: Space filling structures of the frameworks in **CTH-16,** and the isoreticular Gd-btec-MOF with CSD code FEQXAB, with hydrogen atoms omitted.

for systems likely to form compounds that should be very similar or even isostructural. The devil is in the details, different solvents, stoichiometries, and methods yielding these diverse results.

Rod- and sheet-MOF synthesis

Rod-MOF structures may be a strategy for increased stability of MOFs, and btec-type ligands may be a way to achieve that. The vicinal positions of the carboxylates induce chain formation, and the concerted movement of the CO_2^- units (see flexibility discussion) may also be a factor. Experimental indications come from the prominent featuring of btec-MOFs in the 2016 review by Schoedel et al.[2] and also from our analysis of the 43 different REE 3D btec coordination polymers (Table S5). Of these, almost 80% are rod-MOFs, and two are sheet-MOFs. However, due to the shortness of the btec linker, we cannot expect any great porosity or surface area for these.

However, extended btec-type ligands, bridging aromatic ligands with double (such as btec) or triple vicinal carboxylate groups are rare in MOF chemistry. So, while [1,1′:2′,1′′-terphenyl]-4,4′,4′′,5′-tetracarboxylates with one vicinal dicarboxylate are relatively common ligands (36 MOF structures in the CSD), the one benzene group extension of H_4btec to 2,3,6,7-anthracenetetracarboxylic acid has but four known MOF structures.[59]

We see here an opportunity for new families of MOFs: for example, one candidate metal ion being Ce(IV), which we have shown here to be substantially stabilized compared with its aqueous solution chemistry. Ce(IV) MOFs are previously known,[46,60–72] but it is not a large class of MOFs, possibly because of the use of Ce(IV) as a well-known oxidant in organic synthesis. However, Ce(IV) may be more stable than we think,[43,44]

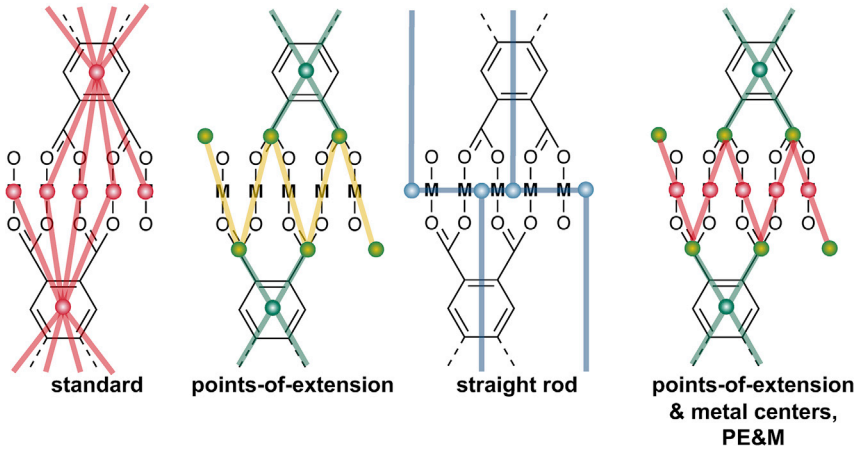

Figure 7. Approaches to rod-MOF topologies

Schematic example of topology approaches for infinite 1D rod-SBUs in btec-MOFs. Left: Node assignment and links according to the TOPOS standard method "standard." Center left: Node assignment and links using the carbonyl carbons as branching points corresponding to the points-of-extension approach. Center right: The straight rod, STR, approach. Right: The points-of-extension & metal centers, PE&M approach.

as we recently noted the spontaneous oxidation of Ce(III) to Ce(IV) forming entities such as $[Fe(III)_4Ce(IV)_4O_4(O_2CCMe_3)_4(N(CH_2CH_2OH)_3)_4(N_3)_4(MeOH)_4]$.[73]

To answer the more general question of whether there are specific conditions favoring rod- and sheet-MOF formation is more difficult. The same parameters that lead to the formation of compounds with non-connected rods and sheets should be good, if these are known. Then, we might just speculate that one difference is that precursors of the dot-MOF may be coordinately saturated discrete 0D metal SBUs that are potentially stable, or meta-stable, in solution. Depending on the stability constants, these may be obtained under high ligand-to-metal ratios. No corresponding solution species are possible for the infinite 1D and 2D metal SBUs of rod- and sheet-MOFs, suggesting that lower ligand-to-metal ratios may be a viable strategy.

Having discussed our results in a broader structural context, we will now look into some specific topology issues.

Network topologies: A unified approach to MOFs

There are three basic approaches for the discussion of the network topologies. The "all-nodes" approach with identification of SBUs, the "standard simplification," which we will simply call "standard," which takes the organic linkers as one node and each metal atom as a separate node thus splitting multinuclear metal SBUs into several nodes, or the "cluster simplification," decomposing the structure into pieces with high connectivity, which may again generate metal SBUs.[14,74,75] The former lends itself more easily to synthesis planning for chemists, whereas the latter two approaches have been coded for, and databases such as the Cambridge Structural Database (CSD) have been searched and analyzed.[14] The topologies reported will be related in a net relation graph[76] and for single-metal SBUs often identical.

For rod-MOFs, the differences are significant (Figure 7). The all-nodes approach has been modified to use the carboxylate carbons as branching points, which has the

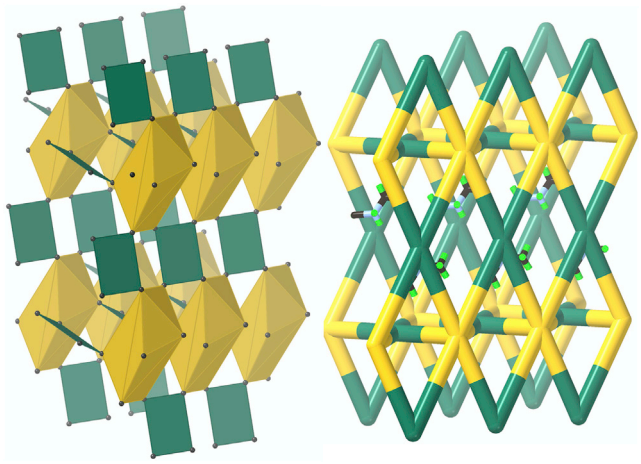

Figure 8. The network in $H_2NMe_2[Y(btec)(H_2O)]$: CTH-14

Left: The form of the metal SBU is two edge-sharing square pyramids depicted as the yellow polyhedral, and the organic SBU is a rectangle shown in green. Right: The resulting network in the all-nodes approach is the eight- (yellow) and four-connected (green) **scu**-net, shown here with the $H_2NMe_2^+$ in the network voids. For the standard approach and the **crg**-net, see Figures S7 and S8.

merit that it will also reflect the shape of the rod. This "points-of-extension" approach[2] is shown in the center left of Figure 7.

Making connections only through the organic ligand does not consider the rod at all (see standard method, Figure 7, left). Recently, alternative approaches to rod-MOFs have been discussed,[16,17] and we will also compare them with a simplified version of the straight rod representation (STR) (Figure 7 center right). We also note the method recently proposed to use both points of extension and metal centers (PE&M, Figure 7 right).[16] This helps avoid some ambiguity in the points-of-extension approach, but it also introduces more nodes.

Topology of $H_2NMe_2[Y(btec)(H_2O)]$: Dot-MOF CTH-14

The coordination network **CTH-14** is a straightforward dot-MOF with the metal SBU as the bridged dimer in the form of two edge-sharing square pyramids (Figure S1), and the structure can be described as eight- and four-connected **scu**-net,[77] with additional space filled with dimethylammonium ions (see Figure 8 right).

Apart from the SBU approach using the dimer as the metal node giving the high symmetry **scu**-net, we could also consider the carboxylates binding to single-metal ions, the standard approach, where we now need to consider Y^{3+} binding to five btec and the btec binding to either 4 or 6 Y^{3+} (Figure S7), but no connection between the two Y^{3+} in the dimer. This gives the 4,5,6-connected net, **crg** (or 4,5,6T11, Figure S8).

The points-of-extension method applied to a dot-MOF

Yet another way of looking at the **CTH-14** structure is to consider the points-of-extension method as used for rod-MOFs. The merit of this would be to have the same description for dot-, rod-, and sheet-MOFs.

We first note that this method has analogies with the augmented net. The augmented net is the net that is formed by replacing nodes by their corresponding polyhedra (Figure 9).[78] This is a common way of depicting, for example, MOF-5 and the **pcu**-net. Thus, the SBU $\{Zn_4O(OCO)_6\}$ in MOF-5 forms an octahedron if we connect the six carbonyl

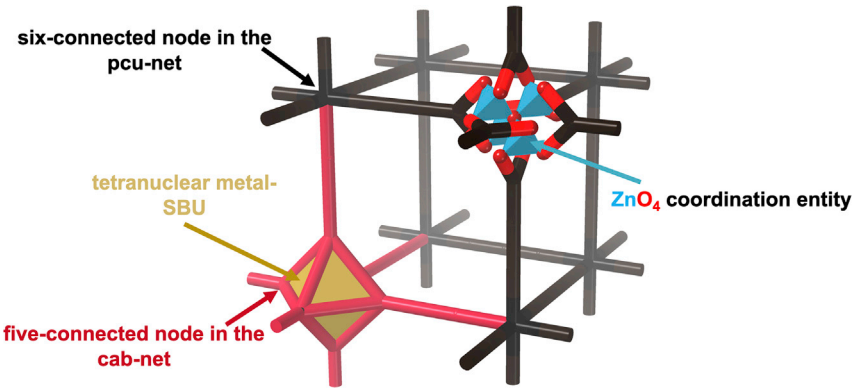

Figure 9. Augmented net and points-of-extension topologies demonstrated in MOF-5
The augmented net is the net that is formed by replacing the nodes by the corresponding coordination figure. This is a common way of depicting, for example, the **pcu**-net and MOF-5. In the picture, we see the six-connected **pcu**-net in black and the augmented five-connected **pcu-a** or **cab**-net in red. We can generalize the augmented net concept and instead use the coordination figure of the actual SBU, which for MOF-5 is identical to the coordination figure of the net. In **CTH-14**, the approach leads to a points-of-extension net.

carbons. In the process, we will also split the 6-connected node of the **pcu**-net into six 5-connected nodes, giving the network topology **cab** or **pcu-a** (-a for augmented).

For the **scu**-net, this means that the **scu-a** is formed by squares and cubes with 3- and 4-connected nodes, respectively. However, other polyhedral shapes can form 8-connected nodes, for example, the two fused square pyramids (Figure S1) that form the metal SBU in **CTH-14**. The points-of-extension net formed in this way is a 6-nodal 4-, 5-, and 6-connected net (with ToposPro designation *loh3*).

Although this may only seem to add unnecessary complications, **pcu** is a perfectly adequate description of MOF-5 and **scu** of **CTH-14**; what the points-of-extension method supplies is a topology including also the metal SBU geometry. This is exactly equivalent to the reported method of analyzing rod-MOFs[2] and also the way we propose to analyze sheet-MOFs.

The points-of-extension method thus puts dot-MOFs, rod-MOFs, and sheet-MOFs on the same topological footing.

Topology of $[Ce_3(btec)(Hbtec)(OAc)(HCO_2)]$: CTH-15

Although MOFs with layered infinite SBUs have been observed before, notably for $[Fe_2(btec)]$ MIL-62,[79] most of these tend to be dense layers, pillared by linkers. Some are based on the corresponding hydroxide structures, such as $[Eu_2(OH)_4(bdc)]$, MIL-51, or the earlier-mentioned ULMOF-1 with a lithium-oxide-based layer. However, the overall shape of a rod is a line, a 1D object, but a 2D infinite SBU may have many overall motifs, like a square planar grid or a honeycomb net. In Figure 10, we can assign a 3-connected honeycomb (**hcb**) motif for the 2D SBU $\{Ce_3(OCO)_7\}^{2-}{}_\infty$ in **CTH-15**. These motifs can, similar to the rods in the rod-MOFs, be constructed in different ways. For example, edge-sharing octahedra may give a honeycomb net.

Using the reported approach for rod-MOFs[2] that we call the points-of-extension method, we take the carboxylate carbons as the points defining the shape of the metal SBU (just as the form of the SBU of MOF-5 is described by an octahedron in Figure 9). This yields chains of edge-sharing trigonal prisms bridged by rectangles

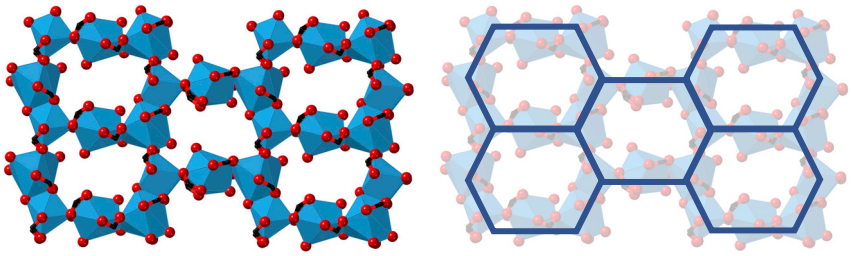

Figure 10. Infinite (sheet) SBU in [Ce_3(btec)(Hbtec)(OAc)(HCO_2)]: CTH-15

The infinite (sheet) SBU in [Ce_3(btec)(Hbtec)(HCO_2)(OAc)] **CTH-15**. Left: Showing Ce and the btec COO^- units. Right: The 2D **hcb** net used for the STR approach. For clarity, bridging btec-nodes or acetates and formates are not shown. See also Figures S9 and S10.

and a three-nodal 4,5,6-connected topology *loh2* (ToposPro designation) with point symbol $\{3^2.4^4.5.6^3\}_2\{3^2.6^4\}\{3^3.4^5.5.6^6\}_2$ (Figure 11).

A similar approach as the standard in Figure 7, linking only metal ions to the centers of the ligands instead gives the edge transitive two-nodal 4- and 6-connected **stp**-net based on square planes and trigonal prisms if we exclude the acetate and formate that can be seen as merely attachments to the network (Figure S10). The straight rod representation can also be extended to 2D with the **hcb**-nets (Figure 10) connected by the btec ligands. If we further simplify by considering the btec ligands as just a link between these sheets, we get the well-known five-connected **bnn**-net (Figure S10).

Compared with the rod-MOFs, these sheet-MOFs seem rare and should by no means be confused with the case of having a flat 0D SBUs forming layers in a structure of a dot-MOF. Two other examples of sheet-MOFs are [$Cd_3(suc)_{2.5}(dpa)_2$]ClO_4 (suc = succinate, dpa = 4,4′-dipyridylamine) with a 8-metal 2D square grid SBU,[80] and [Pb_5(1,3-bdc)$_5(H_2O)_2]_2$ with a 16-metal 2D honeycomb grid SBU with a roughly 5 Å aperture.[81] Because of the extra oxygen enabling the formation of these short

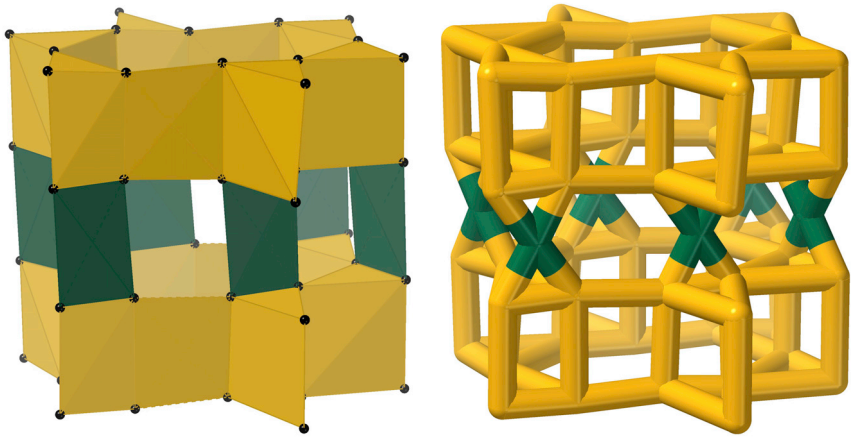

Figure 11. The network in [Ce_3(btec)(Hbtec)(OAc)(HCO_2)]: CTH-15

Left: Polyhedral view with the infinite 2D metal SBU in yellow, defining **CTH-15** as a sheet-MOF, and the bridging btec organic SBU in green. Right: This results in a three-nodal 4,5,6-connected network topology, where btec is 4-connected, as with the points-of-extension method it retains its connectivity irrespective of the detailed layout of the metal coordination.

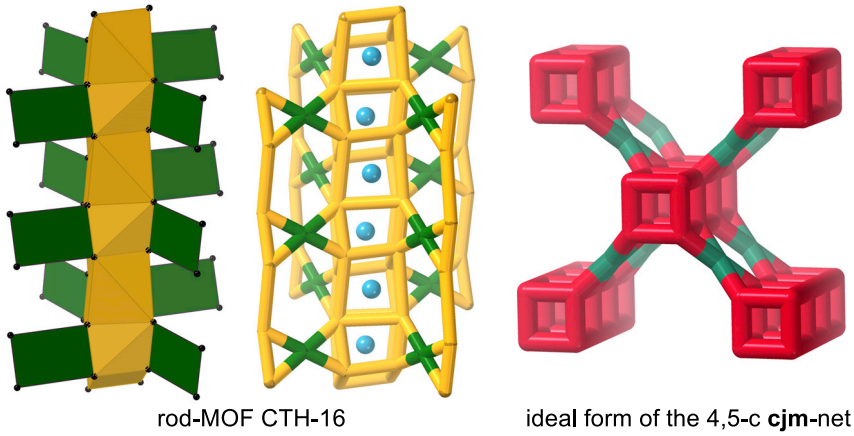

Figure 12. The Gd-btec network in 4,4′-azopyridinium[$Gd_2(btec)_2$]: CTH-16

Left: Polyhedral view with the infinite 1D metal SBU in yellow, defining **CTH-16** as a rod-MOF, and the bridging btec organic SBU in green. The resulting network, center, with Gd^{3+} ions shown as cyan spheres, has a bi-nodal 4,5-connected topology, **cjm** shown in a perpendicular view to the right in its most symmetric form shown. For the standard and STR approaches, see Figure S11.

bridges, one would expect sulfonates and phosphonates[82] to be more prone to form sheet-MOFs, and one such example is $[Co(O_3PC_{14}H_{12}PO_3)].H_2O$.[83]

Topology of 4,4′-azopyridinium[$Gd_2(btec)_2$]: CTH-16

CTH-16, 4,4′-azopyridinium[$Gd_2(btec)_2$] is a typical example of a rod-MOF. The rods are formed by face-sharing cubes, bridged by 4-connecting $btec^{4-}$ ligands, and the points-of-extension approach gives the bi-nodal 4,5-connected topology **cjm** with point symbol $\{3^2.6^2.7^2\}\{3.4^5.5^2.6^2\}_4$ (Figure 12).

The rod-MOF structure **CTH-16** can also be treated with the standard method, yielding the likewise bi-nodal **htp**-net based on hexagons (btec) and trigonal prisms (Gd), the assignment given to the isoreticular 4,4′-bipyridinium[$Ln_2(btec)_2$] compounds in a recent database survey (Figure S4).[14] If we make straight rods and let the btec just be a linear connector, the structure reduces to the **dia**-net in an embedding with seesaw geometry of the nodes (Figure S11).

The merits of the different approaches

In Table 1, we compare some different topology approaches for the compounds presented in this work.

Table 1. Comparison of the different topology approaches

Comp.	All nodes	Points of extension	Standard	Simple STR
MOF-5	**pcu** (*1,1*)	**cab** (*1,2*)	fff (*3,2*)[84]	–
CTH-14 (Y)	**scu** (*2,1*)	loh3[a] (*6,12*)	**crg** (*3,3*)[b]	–
CTH-15 (Ce)	–	loh2[a] (*3,8*)	**stp** (*2,1*)[c]	**bnn** (*1,2*)
CTH-16 (Gd)	–	**cjm** (*2,5*)	**htp** (*2,2*)[5]	**dia** (*1,1*)

Comparison of the different topology approaches for the materials presented in this article and MOF-5 for comparison. For each topology, we also present in parenthesis *p* = number of nodes and *q* = number of edges, as a crude indication of the complexity of each net.

[a]TTD collection code (TOPOS).

[b]TTD code 4,5,6T11

[c]Considering only linking by the btec ligand.

All topology methods have their merits, but it is essential to know the difference, especially for infinite SBUs, and be clear on which one is used. The standard method gives a conceptually simpler way of describing the net (Table 1) but normally has no links in the direction of the rod or the sheet, and thus these become "invisible."

The points-of-extension approach, on the other hand, can easily give very complex rod-SBUs[85] and, we suspect, even more complex sheet-SBUs. One advantage is the preservation, by definition, of the connectivity of the organic SBU. For example, as long as all carboxylate groups of the btec ligand are engaged in metal bonding, btec will always be described as a rectangular 4-connected SBU. Another advantage is the explicit description of the metal SBU that is no longer reduced to a single point.

In addition, the metal SBUs are assembled during the reaction so that planning for a particular network to form, knowledge of what nets are possible with that particular metal SBU, or choosing what metal SBU to aim for will be essential for synthesis planning.

However, one has to be sure that the increased complexity really gives an increased understanding for the points-of-extension approach to be worthwhile. So, although visually picturing MOF-5 as the points-of-extension uninodal net **cab** is closer to the real structure, the topology adds little. The same is true if describing MOF-5 with the three-nodal **fff** topology with the bridging dicarboxylates described as 4-connected nodes in the standard method.

On the other hand, if easy-to-recognize rod or sheet patterns as ladders or fused polyhedra that could inspire the chemist are not what we are after, but instead a numerical comparison of large number of structures, then the PE&M may be a way forward. This gives for MOF-5 the three-nodal **mof**-net. A more detailed description also makes it easier to find closely related materials in various databases.

Conclusions

We have shown that in addition to the common rod-nets there are analogous infinite 2D SBUs forming sheets. We propose that the three classes of MOFs emerging from the designation of the metal SBUs as 0D, 1D, and 2D be called dot-MOFs, rod-MOFs, and sheet-MOFs, respectively, in order for us to be able to discuss them easily.

Bennett and co-workers noted recently that there is a "huge gap in our understanding of the thermal stability of this vast class of materials."[4] Literature data we have assembled, nevertheless, supports the idea that the thermal, but also chemical, stability of MOFs follow in the trend dot < rod < sheet. Certainly, for our materials, the sheet-MOF **CTH-15** was the most stable thermally. Having said that, we want to stress that this is not the only factor determining the stability of a MOF.

The network topologies of all three classes can be analyzed using the points-of-extension method. This does not invalidate or supersede other methods but provides a way of describing all MOFs in the same theoretical framework. Notably, it takes into account the geometry of the metal SBU and preserves the connectivity of the organic SBU.

We suggest that implementing a search algorithm for the points-of-extension method and applying it to the MOF subset in the CSD may yield further insights into MOF structures and properties along the lines of recent studies, with the

standard method, cluster method, or PE&M approaches perhaps more suitable for numerical comparisons.[19]

We have attributed the flexibility, or potential breathing behavior, of **CTH-16** and its isoreticular analogs partly to the large conformational space of the vicinal carboxylates of the btec linker, shown by analysis of data in the CSD.

The photoluminescent behavior suggests potential for further investigations, but most importantly, this was used to identify the guest molecule in **CTH-16**.

Finally, cyclic voltammetry shows a remarkable stabilization of Ce(IV) compared with solution chemistry, and we suggest Ce(III/IV) MOFs to be interesting catalyst candidates for various redox reactions. More experiments are planned to explore the potential for electrochemical redox catalysis with **CTH-15**.

EXPERIMENTAL PROCEDURES

Resource availability

Lead contact

Further information should be directed to and will be fulfilled by the lead contact, Lars Öhrström (ohrstrom@chalmers.se).

Materials availability

All chemicals were purchased from Sigma-Aldrich and were used without further purification. Samples of CTH14-16 may be available on request to the lead contact.

Data and code availability

- Crystallographic Information Files for the structures reported in this paper have been deposited with the Cambridge Crystallographic Data Center (CCDC). The deposition numbers of clusters are CCDC 2019728 (CTH-14), 2088967 (CTH-15), 2019730 (CTH-16) and 2019731 (salt). Copies of the data can be obtained, free of charge, on application to the CCDC, 12 Union Road, Cambridge CB21EZ, U.K. (fax 44 (1223) 336 033; e-mail deposit@ccdc.cam.ac.uk) or on www.ccdc.cam.ac.uk.
- This paper does not report original code.
- Any additional information required to reanalyze the data reported in this paper is available from the lead contact upon request.

Synthesis of CTH-14: (H_2NMe_2)[Y(btec)(H_2O)]

Yttrium nitrate hexahydrate (60.278 mg, 0.157 mmol), 1,2,4,5-benzenetetracarboxylic acid (H_4btec; 20 mg, 0.079 mmol), and 4,4′-azopyridine (4,4′-azpy; 14.495 mg, 0.079 mmol) were dissolved in a 1:1:1 (v/v/v) DMF/H_2O/glacial acetic acid. The reaction mixture was placed in a pyrex tube for solvothermal synthesis at 120°C and colorless crystals which are **CTH-14** were obtained in 24 h. In the same tube, pale yellow crystals, which are a salt formed between H_4btec and the reduced 4,4′-azopyridine; 1,2-di(pyridin-4-yl)hydrazine, were also obtained. **CTH-14** could also be obtained in a similar reaction without the 4,4′-azopyridine. Elemental analysis for **CTH-14**, $C_{12}H_{12}NO_9Y$, calculated (found): C 35.75 (35.23), H 3.00 (2.96), N 3.47 (3.46)%.

Synthesis of (1,2-di(pyridinium-4-yl)hydrazine(H_2btec)), see CTH-14

Synthesis of CTH-15: [Ce_3(btec)(Hbtec)(OAc)(HCO_2)]

Same synthesis procedure was done as for **CTH-14** with the exception that cerium nitrate hexahydrate (68.337 mg, 0.157 mmol) was used, and after 3 days, colorless crystals of **CTH-15** were formed. **CTH-15** could also be obtained in a similar reaction

without the 4,4′-azopyridine. Elemental analysis for **CTH-15** with seven extra water molecules, $C_{23}H_{23}Ce_3O_{27}$, calculated (found): C 23.99 (23.5), H 2.01 (1.9), N 0.4 (0.0)%.

Synthesis of CTH-16: 4,4′-azopyridinium[$Gd_2(btec)_2$]·

The same procedure was followed as in **CTH-14** with the exception that gadolinium nitrate hexahydrate (71.035 mg, 0.079 mmol) was used. Pale yellow crystals were acquired on the second day. Elemental analysis for **CTH-16** with three extra water molecules, $C_{30}H_20Gd_2N_4O_{19}$, calculated (found): C 34.15 (34.39), H 1.91 (2.30), N 5.31 (5.42).

Single-crystal X-ray diffraction

Single-crystal X-ray diffraction data were collected on a Rigaku XtaLAB Synergy-S, Dualflex diffractometer equipped with an AtlasS2 detector at −173°C using Cu Kα radiation (λ = 1.54184 Å) and a Rigaku XtaLAB Synergy-S, Dualflex diffractometer equipped with a HyPix-6000HE detector using Mo Kα radiation (λ = 0.71073 Å). Diffraction data were acquired and processed with CrysAlisPro software package.[86,87] Direct or structure expansion methods were used for all structures, and the refinements were established by full-matrix least squares with SHELX-2018/3[88] using X-seed[89] and Olex2[90] software as a graphical interface. Details of structure refinements are found in the supplemental information.

Volumetric gas adsorption and surface area analysis

N_2 adsorption isotherms were recorded on a Micromeritics ASAP2020 surface area analyzer at liquid N_2 temperature (−196°C). The samples were pre-treated at 120°C under dynamic vacuum (1×10^{-4} Pa) for 6 h before the analysis. The relative pressure range of 0.05–0.15 was used to estimate the Langmuir and BET surface area of the samples. Additionally, CO_2 and N_2 adsorption isotherms were recorded at 20°C (with a temperature-controlled water bath) using the same instrument.

Cyclic voltammetry

All electrochemical measurements were made in a three-electrode cell with an Ag/AgCl reference electrode and a Pt mesh counter electrode. The working electrode consisted of carbon paste (Metrohm), with and without electroactive material. The composition of the electroactive part was 50/50 wt % of carbon paste and electroactive material. A phosphate buffer with pH = 7 and concentration 0.1 M was used as electrolyte. The electrolyte was purged with nitrogen before each experiment, and a stream of nitrogen was kept over the solution during the experiments. The scan rate was 10 mV/s.

Emission measurements

Room temperature steady-state emission spectra of the compounds were obtained with a Spex Fluorolog 3 from JY Horiba; the excitation wavelength was 300 nm for all samples. For H_4btec, 4,4′-azopyridine, **CTH-15**, and **CTH-16**, the samples were loaded into 1-mm cuvettes, but for **CTH-14**, the sample was deposited on a glass substrate, as there was not enough to fill a cuvette.

SUPPLEMENTAL INFORMATION

Supplemental information can be found online at https://doi.org/10.1016/j.chempr.2021.07.006.

ACKNOWLEDGMENTS

We thank Ms. Michelle Åhlén for assistance with the stability studies, Ms. Elin Sundin for assistance with the emission measurements, and Chalmers Materials Analysis Laboratory for assistance with elemental analysis. We are also grateful to the Swedish Research Council (F.M.A.N. and L.Ö., 2017-04725), the Carlsberg Foundation (C.J.M., CF15-0675), Professor M. O'Keeffe for adding **crg** and **cjm** to the RCSR, and Professor V. Blatov for adding *loh2* and *loh3* to the TTD collection. We thank Professor O.M. Yaghi for discussions on the dot-, rod-, and sheet-MOF concept.

AUTHOR CONTRIBUTIONS

Conceptualization, F.M.A.N. and L.Ö.; methodology, F.M.A.N. and L.Ö.; investigation, F.M.A.N., E.A., O.C., C.J.M., C.R.G., M.A., and L.Ö.; writing – original draft, F.M.A.N., E.A., and L.Ö.; writing – review & editing, F.M.A.N., M.A., E.A., O.C., C.J.M., C.R.G., and L.Ö.; funding acquisition, L.Ö.; resources, L.Ö., M.A., C.J.M., and E.A.

DECLARATION OF INTERESTS

The authors declare no competing interests.

INCLUSION AND DIVERSITY

One or more of the authors of this paper self-identifies as an underrepresented ethnic minority in science.

Received: December 12, 2020
Revised: January 27, 2021
Accepted: July 13, 2021
Published: August 9, 2021

REFERENCES

1. Yaghi, O.M., Kalmutzki, M.J., and Diercks, C.S. (2019). Introduction to Reticular Chemistry - Metal-Organic Frameworks and Covalent Organic Frameworks (Wiley-VCH).

2. Schoedel, A., Li, M., Li, D., O'Keeffe, M., and Yaghi, O.M. (2016). Structures of metal-organic frameworks with rod secondary building units. Chem. Rev. *116*, 12466–12535. https://doi.org/10.1021/acs.chemrev.6b00346.

3. Ding, M.L., Cai, X.C., and Jiang, H.L. (2019). Improving MOF stability: approaches and applications. Chem. Sci. *10*, 10209–10230. https://doi.org/10.1039/c9sc03916c.

4. Healy, C., Patil, K.M., Wilson, B.H., Hermanspahn, L., Harvey-Reid, N.C., Howard, B.I., Kleinjan, C., Kolien, J., Payet, F., Telfer, S.G., et al. (2020). The thermal stability of metal-organic frameworks. Coord. Chem. Rev. *419*, 213388. https://doi.org/10.1016/j.ccr.2020.213388.

5. Hanikel, N., Prévot, M.S., Fathieh, F., Kapustin, E.A., Lyu, H., Wang, H., Diercks, N.J., Glover, T.G., and Yaghi, O.M. (2019). Rapid cycling and exceptional yield in a metal-organic framework water harvester. ACS Cent. Sci. *5*, 1699–1706. https://doi.org/10.1021/acscentsci.9b00745.

6. Briggs, L., Newby, R., Han, X., Morris, C.G., Savage, M., Krap, C.P., Easun, T.L., Frogley, M.D., Cinque, G., Murray, C.A., et al. (2021). Binding and separation of CO_2, SO2 and C2H2 in homo- and hetero-metallic metal–organic framework materials. J. Mater. Chem. A *9*, 7190–7197. https://doi.org/10.1039/D1TA00687H.

7. Banerjee, D., Kim, S.J., and Parise, J.B. (2009). Lithium based metal−organic framework with exceptional stability. Cryst. Growth Des. *9*, 2500–2503. https://doi.org/10.1021/cg8014157.

8. Siman, P., Trickett, C.A., Furukawa, H., and Yaghi, O.M. (2015). l-aspartate links for stable sodium metal–organic frameworks. Chem. Commun. (Camb) *51*, 17463–17466. https://doi.org/10.1039/C5CC07578E.

9. Öhrström, L. (2016). Designing, describing and disseminating new materials by using the network topology approach. Chemistry *22*, 13758–13763. https://doi.org/10.1002/chem.201602534.

10. Chung, Y.G., Haldoupis, E., Bucior, B.J., Haranczyk, M., Lee, S., Zhang, H., Vogiatzis, K.D., Milisavljevic, M., Ling, S., Camp, J.S., et al. (2019). Advances, updates, and analytics for the computation-ready, experimental metal–organic framework database: CoRE MOF 2019. J. Chem. Eng. Data *64*, 5985–5998. https://doi.org/10.1021/acs.jced.9b00835.

11. Robson, R. (2000). A net-based approach to coordination polymers. J. Chem. Soc. Dalton Trans. (21), 3735–3744. https://doi.org/10.1039/b003591m.

12. Wells, A.F. (1977). Three-Dimensional Nets and Polyhedra (John Wiley & Sons).

13. Alexandrov, E.V., Blatov, V.A., Kochetkov, A.V., and Proserpio, D.M. (2011). Underlying nets in three-periodic coordination polymers: topology, taxonomy and prediction from a computer-aided analysis of the Cambridge Structural Database. CrystEngComm *13*, 3947–3958. https://doi.org/10.1039/c0ce00636j.

14. Shevchenko, A.P., Alexandrov, E.V., Golov, A.A., Blatova, O.A., Duyunova, A.S., and Blatov, V.A. (2020). Topology versus porosity: what can reticular chemistry tell us about free space in metal-organic frameworks? Chem. Commun. (Camb) *56*, 9616–9619. https://doi.org/10.1039/D0CC04004E.

15. Amombo Noa, F.M., Svensson Grape, E., Brülls, S.M., Cheung, O., Malmberg, P., Inge, A.K., McKenzie, C.J., Mårtensson, J., and Öhrström, L. (2020). Metal–organic frameworks with Hexakis(4-carboxyphenyl)benzene: extensions to reticular chemistry and introducing foldable nets. J. Am. Chem. Soc.

142, 9471–9481. https://doi.org/10.1021/jacs.0c02984.

16. Xie, L.S., Alexandrov, E.V., Skorupskii, G., Proserpio, D.M., and Dincă, M. (2019). Diverse π–π stacking motifs modulate electrical conductivity in tetrathiafulvalene-based metal–organic frameworks. Chem. Sci. *10*, 8558–8565. https://doi.org/10.1039/C9SC03348C.

17. Tshuma, P., Makhubela, B.C.E., Öhrström, L., Bourne, S.A., Chatterjee, N., Beas, I.N., Darkwa, J., and Mehlana, G. (2020). Cyclometalation of lanthanum(iii) based MOF for catalytic hydrogenation of carbon dioxide to formate. RSC Adv *10*, 3593–3605. https://doi.org/10.1039/C9RA09938G.

18. Alexandrov, E.V., Shevchenko, A.P., and Blatov, V.A. (2019). Topological databases: why do we need them for design of coordination polymers? Cryst. Growth Des. *19*, 2604–2614. https://doi.org/10.1021/acs.cgd.8b01721.

19. Shevchenko, A.P., and Blatov, V.A. (2021). Simplify to understand: how to elucidate crystal structures? Struct. Chem. *32*, 507–519. https://doi.org/10.1007/s11224-020-01724-4.

20. Saraci, F., Quezada-Novoa, V., Donnarumma, P.R., and Howarth, A.J. (2020). Rare-earth metal–organic frameworks: from structure to applications. Chem. Soc. Rev. *49*, 7949–7977. https://doi.org/10.1039/D0CS00292E.

21. Jang, S., Song, S., Lim, J.H., Kim, H.S., Phan, B.T., Ha, K., Park, S., and Park, K.H. (2020). Application of various metal-organic frameworks (MOFs) as catalysts for air and water pollution environmental remediation. Catalysts *10*. ARTN 195. https://doi.org/10.3390/catal10020195.

22. Sun, W., Li, X., Sun, C., Huang, Z., Xu, H., and Shen, W. (2019). Insights into the pyrolysis processes of Ce-MOFs for preparing highly active catalysts of toluene combustion. Catalysts *9*. ARTN 682. https://doi.org/10.3390/catal9080682.

23. Liu, J., Redfern, L.R., Liao, Y., Islamoglu, T., Atilgan, A., Farha, O.K., and Hupp, J.T. (2019). Metal–organic-framework-supported and -Isolated ceria clusters with mixed oxidation states. ACS Appl. Mater. Interfaces *11*, 47822–47829. https://doi.org/10.1021/acsami.9b12261.

24. Yaghi, O.M., Li, H., and Groy, T.L. (1997). Crystal structure of 1,2,4,5-benzenetetracarboxylate monohydrate cerium(III) $C_{10}H_4CeO_9$. Z Kristallogr *212*, 457–458. https://doi.org/10.1524/ncrs.1997.212.1.457.

25. Thommes, M., Kaneko, K., Neimark, A.V., Olivier, J.P., Rodriguez-Reinoso, F., Rouquerol, J., and Sing, K.S.W. (2015). Physisorption of gases, with special reference to the evaluation of surface area and pore size distribution (IUPAC Technical Report). Pure Appl. Chem. *87*, 1051–1069. https://doi.org/10.1515/pac-2014-1117.

26. Wang, Y.-B., Zhuang, W.-J., Jin, L.-P., and Lu, S.-Z. (2005). New lanthanide coordination polymers of 1,2,4,5-benzenetetracarboxylic acid and 4,4′-bipyridine with 1D channels. J. Mol. Struct. *737*, 165–172. https://doi.org/10.1016/j.molstruc.2004.10.062.

27. Theilmann, O., Saak, W., Haase, D., and Beckhaus, R. (2009). Reactions of Low-Valent titanocene(II) fragments with trans -4,4′-Azobispyridine (RN=NR, R = C5H4N): formation of tetranuclear molecular squares by trans − cis isomerization. Organometallics *28*, 2799–2807. https://doi.org/10.1021/om801123k.

28. Li, S., Limbach, R., Longley, L., Shirzadi, A.A., Walmsley, J.C., Johnstone, D.N., Midgley, P.A., Wondraczek, L., and Bennett, T.D. (2019). Mechanical properties and processing techniques of bulk metal-organic framework glasses. J. Am. Chem. Soc. *141*, 1027–1034. https://doi.org/10.1021/jacs.8b11357.

29. Lee, S., Kapustin, E.A., and Yaghi, O.M. (2016). Coordinative alignment of molecules in chiral metal-organic frameworks. Science *353*, 808–811. https://doi.org/10.1126/science.aaf9135.

30. Öhrström, L., and Amombo Noa, F.M. (2021). Metal-Organic Fameworks. (American Chemical Society). https://doi.org/10.1021/acs.infocus.7e4004.

31. Cañadillas-Delgado, L., Fabelo, O., Pasán, J., Delgado, F.S., Lloret, F., Julve, M., and Ruiz-Pérez, C. (2010). Intramolecular ferro- and antiferromagnetic interactions in oxo-carboxylate bridged digadolinium(iii) complexes. Dalton Trans *39*, 7286–7293. https://doi.org/10.1039/B920156D.

32. Hashimoto, M., Igawa, S., Yashima, M., Kawata, I., Hoshino, M., and Osawa, M. (2011). Highly efficient green organic light-emitting diodes containing luminescent three-coordinate copper(I) complexes. J. Am. Chem. Soc. *133*, 10348–10351. https://doi.org/10.1021/ja202965y.

33. Kent, C.A., Liu, D., Meyer, T.J., and Lin, W. (2012). Amplified luminescence quenching of phosphorescent metal–organic frameworks. J. Am. Chem. Soc. *134*, 3991–3994. https://doi.org/10.1021/ja211271m.

34. Ju, P., Zhang, E.-s., Liu, X., and Jiang, L. (2020). Two novel 3D MOFs based on the flexible (E)-1,4-di(1H-imidazol-1-yl)but-2-ene and multi-carboxylate ligands: synthesis, structural diversity and luminescence property. Inorg. Chem. Commun. *111*, 107641. https://doi.org/10.1016/j.inoche.2019.107641.

35. Li, X.H., Wang, Y.P., Ma, Z.Y., Zhang, R.L., and Zhao, J.S. (2010). Synthesis and characterization of two 3-D polymeric lanthanide complexes constructed from 1,2,4,5-benzenetetracarboxylic acid. J. Coord. Chem. *63*, 1029–1037. https://doi.org/10.1080/00958971003690439.

36. Gai, Y.-L., Jiang, F.-L., Xiong, K.-C., Chen, L., Yuan, D.-Q., Zhang, L.-J., Zhou, K., and Hong, M.-C. (2012). Temperature-dependent in situ reduction of 4,4′-Azobispyridine via solvothermal reaction. Cryst. Growth Des. *12*, 2079–2088. https://doi.org/10.1021/cg3000813.

37. Bünzli, J.-C.G., and Eliseeva, S.V. (2011). Basics of lanthanide photophysics. In Lanthanide Luminescence: Photophysical, Analytical and Biological Aspects, P. Hänninen and H. Härmä, eds. (Springer), pp. 1–45. https://doi.org/10.1007/4243_2010_3.

38. Zhu, Y., Wang, L., Chen, X., Wang, P., Fan, Y., and Zhang, P. (2017). 3D lanthanide metal-organic frameworks constructed from 2,6-naphthalenedicarboxylate ligand: synthesis, structure, luminescence and dye adsorption. J. Solid State Chem. *251*, 248–254. https://doi.org/10.1016/j.jssc.2017.04.026.

39. Pladzyk, A., Ponikiewski, Ł., Dołęga, A., Słowy, K., Sokołowska, A., Dziubińska, K., and Hnatejko, Z. (2015). Structural variety of cobalt(II), nickel(II), zinc(II), and cadmium(II) complexes with 4,4′-Azopyridine: synthesis, structure and luminescence properties. Chem. Asian J. *10*, 2388–2396. https://doi.org/10.1002/asia.201500652.

40. Kaur, H., Sundriyal, S., Pachauri, V., Ingebrandt, S., Kim, K.H., Sharma, A.L., and Deep, A. (2019). Luminescent metal-organic frameworks and their composites: potential future materials for organic light emitting displays. Coord. Chem. Rev. *401*, 213077. https://doi.org/10.1016/j.ccr.2019.213077.

41. Gutiérrez, M., Martin, C., Kennes, K., Hofkens, J., Van der Auweraer, M., Sánchez, F., and Douhal, A. (2018). New OLEDs based on zirconium metal-organic framework. Adv. Opt. Mater. *6*, 1701060. https://doi.org/10.1002/adom.201701060.

42. CRC Handbook of Chemistry and Physics. (2020). 101 Edition (CRC Press, Inc.)..

43. Haraguchi, N., Okaue, Y., Isobe, T., and Matsuda, Y. (1994). Stabilization of tetravalent cerium upon coordination of unsaturated heteropolytungstate anions. Inorg. Chem. *33*, 1015–1020. https://doi.org/10.1021/ic00084a008.

44. Piro, N.A., Robinson, J.R., Walsh, P.J., and Schelter, E.J. (2014). The electrochemical behavior of cerium(III/IV) complexes: thermodynamics, kinetics and applications in synthesis. Coord. Chem. Rev. *260*, 21–36. https://doi.org/10.1016/j.ccr.2013.08.034.

45. Deblonde, G.J.P., Sturzbecher-Hoehne, M., and Abergel, R.J. (2013). Solution thermodynamic stability of complexes formed with the octadentate hydroxypyridinonate ligand 3,4,3-LI(1,2-HOPO): a critical feature for efficient chelation of lanthanide(IV) and actinide(IV) ions. Inorg. Chem. *52*, 8805–8811. https://doi.org/10.1021/ic4010246.

46. Shen, C.H., Chuang, C.H., Gu, Y.J., Ho, W.H., Song, Y.D., Chen, Y.C., Wang, Y.C., and Kung, C.W. (2021). Cerium-based metal–organic framework nanocrystals interconnected by carbon nanotubes for boosting electrochemical capacitor performance. ACS Appl. Mater. Interfaces *13*, 16418–16426. https://doi.org/10.1021/acsami.1c02038.

47. Arenas, L.F., Ponce de León, C., and Walsh, F.C. (2016). Electrochemical redox processes involving soluble cerium species. Electrochim. Acta *205*, 226–247. https://doi.org/10.1016/j.electacta.2016.04.062.

48. Tajik, S., Beitollahi, H., Nejad, F.G., Kirlikovali, K.O., Van Le, Q.V., Jang, H.W., Varma, R.S., Farha, O.K., and Shokouhimehr, M. (2020). Recent electrochemical applications of metal-organic framework-based materials. Cryst. Growth Des. *20*, 7034–7064. https://doi.org/10.1021/acs.cgd.0c00601.

49. Garcia-Segura, S., Lanzarini-Lopes, M., Hristovski, K., and Westerhoff, P. (2018). Electrocatalytic reduction of nitrate: fundamentals to full-scale water treatment applications. Appl. Catal. B *236*, 546–568. https://doi.org/10.1016/j.apcatb.2018.05.041.

50. Zeng, Y.C., Priest, C., Wang, G.F., and Wu, G. (2020). Restoring the nitrogen cycle by electrochemical reduction of nitrate: progress and prospects. Small Methods *4*, 2000672. https://doi.org/10.1002/smtd.202000672.

51. Wang, L.Q., Zhu, Y.Q., Du, C.L., Ma, X.L., and Cao, C.B. (2020). Advances and challenges in metal-organic framework derived porous materials for batteries and electrocatalysis. J. Mater. Chem. A *8*, 24895–24919. https://doi.org/10.1039/D0TA08311A.

52. Meza-Pardo, I.G., Morales-Tapia, A.A., Veloz Rodríguez, M.A., Reyes-Cruz, V.E., Perez-Labra, M., Urbano-Reyes, G., Rivera-Villanueva, J.M., and Cobos-Murcia, J.A. (2020). Synthesis of UV-11 MOF and its characterization by cyclic voltammetry. Front. Chem. *8*, 617. https://doi.org/10.3389/fchem.2020.00617.

53. Férey, G., and Serre, C. (2009). Large breathing effects in three-dimensional porous hybrid matter: facts, analyses, rules and consequences. Chem. Soc. Rev. *38*, 1380–1399. https://doi.org/10.1039/B804302G.

54. Schneemann, A., Bon, V., Schwedler, I., Senkovska, I., Kaskel, S., and Fischer, R.A. (2014). Flexible metal–organic frameworks. Chem. Soc. Rev. *43*, 6062–6096. https://doi.org/10.1039/C4CS00101J.

55. Bon, V., Kavoosi, N., Senkovska, I., and Kaskel, S. (2015). Tolerance of flexible MOFs toward repeated adsorption stress. ACS Appl. Mater. Interfaces *7*, 22292–22300. https://doi.org/10.1021/acsami.5b05456.

56. Wei, Y.-S., Chen, K.-J., Liao, P.-Q., Zhu, B.-Y., Lin, R.-B., Zhou, H.-L., Wang, B.-Y., Xue, W., Zhang, J.-P., and Chen, X.-M. (2013). Turning on the flexibility of isoreticular porous coordination frameworks for drastically tunable framework breathing and thermal expansion. Chem. Sci. *4*, 1539–1546. https://doi.org/10.1039/C3SC22222E.

57. Alexandrov, E.V., Goltsev, A.V., Eremin, R.A., and Blatov, V.A. (2019). Anisotropy of elastic properties of metal-organic frameworks and the breathing phenomenon. J. Phys. Chem. C *123*, 24651–24658. https://doi.org/10.1021/acs.jpcc.9b08434.

58. Parent, L.R., Pham, C.H., Patterson, J.P., Denny, M.S., Cohen, S.M., Gianneschi, N.C., and Paesani, F. (2017). Pore breathing of metal–organic frameworks by environmental transmission electron microscopy. J. Am. Chem. Soc. *139*, 13973–13976. https://doi.org/10.1021/jacs.7b06585.

59. Chang, Z., Zhang, A.-S., Hu, T.-L., and Bu, X.-H. (2009). ZnII coordination Poylmers based on 2,3,6,7-Anthracenetetracarboxylic acid: synthesis, structures, and luminescence properties. Cryst. Growth Des *9*, 4840–4846. https://doi.org/10.1021/cg900659r.

60. Lammert, M., Glißmann, C., Reinsch, H., and Stock, N. (2017). Synthesis and characterization of new Ce(IV)-MOFs exhibiting various framework topologies. Cryst. Growth Des. *17*, 1125–1131. https://doi.org/10.1021/acs.cgd.6b01512.

61. Dalapati, R., Sakthivel, B., Dhakshinamoorthy, A., Buragohain, A., Bhunia, A., Janiak, C., and Biswas, S. (2016). A highly stable dimethyl-functionalized Ce(IV)-based UiO-66 metal-organic framework material for gas sorption and redox catalysis. CrystEngComm *18*, 7855–7864. https://doi.org/10.1039/C6CE01704E.

62. Dalapati, R., Sakthivel, B., Ghosalya, M.K., Dhakshinamoorthy, A., and Biswas, S. (2017). A cerium-based metal-organic framework having inherent oxidase-like activity applicable for colorimetric sensing of biothiols and aerobic oxidation of thiols. CrystEngComm *19*, 5915–5925. https://doi.org/10.1039/C7CE01053B.

63. Heidenreich, N., Waitschat, S., and Reinsch, H. (2018). Investigation of the kinetic stabilization of a Ce4+-based MOF by in-situ powder X-ray diffraction. Z. Anorg. Allg. Chem. *644*, 1826–1831. https://doi.org/10.1002/zaac.201800354.

64. Jacobsen, J., Wegner, L., Reinsch, H., and Stock, N. (2020). Ce-MIL-140: expanding the synthesis routes for cerium(IV) metal-organic frameworks. Dalton Trans *49*, 11396–11402. https://doi.org/10.1039/d0dt02455d.

65. Lammert, M., Glissmann, C., and Stock, N. (2017). Tuning the stability of bimetallic Ce((IV))/Zr((IV))-based MOFs with UiO-66 and MOF-808 structures. Dalton Trans *46*, 2425–2429. https://doi.org/10.1039/c7dt00259a.

66. Luo, L.P., Huang, L.J., Liu, X.N., Zhang, W.T., Yao, X.L., Dou, L.N., Zhang, X., Nian, Y., Sun, J., and Wang, J.L. (2019). Mixed-valence Ce-BPyDC metal-organic framework with dual enzyme-like activities for colorimetric biosensing. Inorg. Chem. *58*, 11382–11388. https://doi.org/10.1021/acs.inorgchem.9b00661.

67. Matemb Ma Ntep, T.J., Reinsch, H., Liang, J., and Janiak, C. (2019). Acetylenedicarboxylate-based cerium(IV) metal-organic framework with fcu topology: a potential material for air cleaning from toxic halogen vapors. Dalton Trans *48*, 15849–15855. https://doi.org/10.1039/c9dt03518d.

68. Sangeetha, S., and Krishnamurthy, G. (2020). Electrochemical and photocatalytic applications of Ce-MOF. Bull. Mater. Sci. *43*, 269. https://doi.org/10.1007/s12034-020-02225-0.

69. Smolders, S., Lomachenko, K.A., Bueken, B., Struyf, A., Bugaev, A.L., Atzori, C., Stock, N., Lamberti, C., Roeffaers, M.B.J., and De Vos, D.E. (2018). Unravelling the redox-catalytic behavior of Ce4+ metal-organic frameworks by X-ray absorption spectroscopy. ChemPhysChem *19*, 373–378. https://doi.org/10.1002/cphc.201700967.

70. Yu, H., Han, J., An, S.J., Xie, G., and Chen, S.P. (2018). Ce(III, IV)-MOF electrocatalyst as signal-amplifying tag for sensitive electrochemical aptasensing. Biosens. Bioelectron. *109*, 63–69. https://doi.org/10.1016/j.bios.2018.03.005.

71. Zhou, J.J., Liu, H., Lin, Y.C., Zhou, C., and Huang, A.S. (2020). Synthesis of well-shaped and high-crystalline Ce-based metal organic framework for CO_2/CH4 separation. Micropor. Mesopor. Mater. *302*, 110224. https://doi.org/10.1016/j.micromeso.2020.110224.

72. Jacobsen, J., Ienco, A., D'Amato, R., Costantino, F., and Stock, N. (2020). The chemistry of Ce-based metal–organic frameworks. Dalton Trans *49*, 16551–16586. https://doi.org/10.1039/D0DT02813D.

73. Baca, S.G., Amombo Noa, F.M., and Öhrström, L. (2021). Octanuclear heterometallic FeIII-CeIV pivalate clusters: from a close {Fe4Ce4(μ4-O)4} cage to an open {Fe4Ce4(μ4-O)2(μ3-O)2} core. Inorg. Chim. Acta *515*, 120038. https://doi.org/10.1016/j.ica.2020.120038.

74. Blatov, V.A., Shevchenko, A.P., and Proserpio, D.M. (2014). Applied topological analysis of crystal structures with the program package ToposPro. Cryst. Growth Des. *14*, 3576–3586. https://doi.org/10.1021/cg500498k.

75. Bonneau, C., O'Keeffe, M., Proserpio, D.M., Blatov, V.A., Batten, S.R., Bourne, S.A., Lah, M.S., Eon, J.-G., Hyde, S.T., Wiggin, S.B., and Öhrström, L. (2018). Deconstruction of crystalline networks into underlying nets: relevance for terminology guidelines and crystallographic databases. Cryst. Growth Des. *18*, 3411–3418. https://doi.org/10.1021/acs.cgd.8b00126.

76. Blatov, V.A., Golov, A.A., Yang, C., Zeng, Q., and Kabanov, A.A. (2019). Network topological model of reconstructive solid-state transformations. Sci. Rep. *9*, 6007. https://doi.org/10.1038/s41598-019-42483-5.

77. Borel, C., Håkansson, M., and Öhrström, L. (2006). Coordination bonds and strong hydrogen bonds giving a framework material based on a 4-and 8-connected net in [Ca [Co(en)(oxalato)2]2]n. Crystengcomm *8*, 666–669. https://doi.org/10.1039/b605762d.

78. O'Keeffe, M. (2014). Nets, tiles, and metal-organic frameworks. APL Mater *2*, 124106. https://doi.org/10.1063/1.4901292.

79. Sanselme, M., Grenèche, J.M., Riou-Cavellec, M., and Férey, G. (2002). [Fe2(C10O8H2) An Antiferromagnetic 3D Iron(II) Carboxylate Built from Ferromagnetic Edge-Sharing Octahedral Chains (MIL-62)]. Chem. Commun. *2002*, 2172–2173.

80. Shyu, E., and LaDuca, R.L. (2009). Divalent metal succinate/perchlorate coordination polymers incorporating a kinked hydrogen-bonding capable diimine: chains, layers and a (5,6)-connected binodal network featuring alternating rectangular and hexagonal grids. Polyhedron *28*, 826–834. https://doi.org/10.1016/j.poly.2008.12.026.

81. Zhang, L., Li, Z.J., Lin, Q.P., Qin, Y.Y., Zhang, J., Yin, P.X., Cheng, J.K., and Yao, Y.G. (2009). Synthesis, structure, and luminescent properties of hybrid inorganic−organic framework materials formed by lead aromatic carboxylates: inorganic connectivity variation from 0D to 3D. Inorg. Chem. *48*, 6517–6525. https://doi.org/10.1021/ic900425r.

82. Shimizu, G.K.H., Vaidhyanathan, R., and Taylor, J.M. (2009). Phosphonate and sulfonate metal organic frameworks. Chem. Soc. Rev. *38*, 1430–1449. https://doi.org/10.1039/B802423P.

83. Parnham, E.R., Drylie, E.A., Wheatley, P.S., Slawin, A.M.Z., and Morris, R.E. (2006). Ionothermal materials synthesis using unstable

deep-eutectic solvents as template-delivery agents. Angew. Chem. Int. Ed. Engl. *45*, 4962–4966. https://doi.org/10.1002/anie.200600290.

84. Barthel, S., Alexandrov, E.V., Proserpio, D.M., and Smit, B. (2018). Distinguishing metal–organic frameworks. Cryst. Growth Des. *18*, 1738–1747. https://doi.org/10.1021/acs.cgd.7b01663.

85. Inge, A.K., Köppen, M., Su, J., Feyand, M., Xu, H.Y., Zou, X.D., O'Keeffe, M., and Stock, N. (2016). Unprecedented topological complexity in a metal-organic framework constructed from simple building units. J. Am. Chem. Soc. *138*, 1970–1976. https://doi.org/10.1021/jacs.5b12484.

86. Agilent Technologies (2005). Crysalis CCD (Oxford Diffraction Ltd.).

87. Agilent Technologies (2005). Crysalis RED (Oxford Diffraction Ltd.).

88. Sheldrick, G.M. (2015). Crystal structure refinement with SHELXL. Acta Crystallogr. C Struct. Chem. *71*, 3–8. https://doi.org/10.1107/S2053229614024218.

89. Barbour, L.J. (2020). X-seed 4: updates to a program for small-molecule supramolecular crystallography. J. Appl. Crystallogr. *53*, 1141–1146. https://doi.org/10.1107/S1600576720007438.

90. Dolomanov, O.V., Bourhis, L.J., Gildea, R.J., Howard, J.A.K., and Puschmann, H. (2009). OLEX2: a complete structure solution, refinement and analysis program. J. Appl. Crystallogr. *42*, 339–341. https://doi.org/10.1107/S0021889808042726.